ARL-TR-10388 ● JULY 2026

Fast Charging of 3000- and 3500-mAh Lithium-Ion Batteries Using a Sinusoidal Ripple Current Method

by Richard L. Thomas Jr.

NOTICES

Disclaimers

ARL-TR-10388 ● JULY 2026

Fast Charging of 3000- and 3500-mAh Lithium-Ion Batteries Using a Sinusoidal Ripple Current Method

Richard L. Thomas Jr.
DEVCOM Army Research Laboratory

REPORT DOCUMENTATION PAGE

1. REPORT DATE	2. REPORT TYPE	3. DATES COVERED START DATE	3. DATES COVERED END DATE
July 2026	Technical Report	1 January 2024	2 September 2024

4. TITLE AND SUBTITLE
Fast Charging of 3000- and 3500-mAh Lithium-Ion Batteries Using a Sinusoidal Ripple Current Method

5a. CONTRACT NUMBER	5b. GRANT NUMBER	5c. PROGRAM ELEMENT NUMBER
5d. PROJECT NUMBER	**5e. TASK NUMBER**	**5f. WORK UNIT NUMBER**

6. AUTHOR(S)
Richard L. Thomas Jr.

7. PERFORMING ORGANIZATION NAME(S) AND ADDRESS(ES)	8. PERFORMING ORGANIZATION REPORT NUMBER
DEVCOM Army Research Laboratory ATTN: FCDD-RLA-GD Adelphi, MD 20783-1138	ARL-TR-10388

9. SPONSORING/MONITORING AGENCY NAME(S) AND ADDRESS(ES)	10. SPONSOR/MONITOR'S ACRONYM(S)	11. SPONSOR/MONITOR'S REPORT NUMBER(S)

12. DISTRIBUTION/AVAILABILITY STATEMENT
DISTRIBUTION STATEMENT A. Approved for public release: distribution unlimited.

13. SUPPLEMENTARY NOTES

14. ABSTRACT
The U.S. Army is interested in fast charging the most energy-dense lithium-ion batteries (LIBs) currently available—i.e., 18650 size with an Ampere hour (Ah) rating between 3.0 and 3.5 Ah. The common charging method currently used is a constant current–constant voltage (CC-CV) method that is very effective for nominal charging and usually takes about 1.5 h or more to achieve a 100% charge. When CC-CV charging is used for faster charging of LIBs (i.e., at twice the standard charging rate), studies and common understanding suggest it can reduce battery lifespan. Specifically, some sources indicate that when a battery's State of Health (SOH) is down to 80%, using fast charging can cause significant life-cycle reduction, with some studies suggesting a reduction of approximately 75%. In this report, the CC-CV charging method will be compared with the sinusoidal ripple current average constant voltage method. To evaluate this method the rate of charge will be three times the nominal charging rate for the LIBs under test, which equates to 3 C for 3000-mAh LIBs and 1.5 C for 3300- and 3500-mAh LIBs.

15. SUBJECT TERMS
fast charging, sinusoidal method, lithium ion, 18650 cell

16. SECURITY CLASSIFICATION OF: a. REPORT	b. ABSTRACT	C. THIS PAGE	17. LIMITATION OF ABSTRACT	18. NUMBER OF PAGES
UNCLASSIFIED	UNCLASSIFIED	UNCLASSIFIED	UU	27

19a. NAME OF RESPONSIBLE PERSON	19b. PHONE NUMBER *(Include area code)*
Richard L. Thomas Jr.	(520) 691-5665

STANDARD FORM 298 (REV. 5/2020)
Prescribed by ANSI Std. Z39.18

Contents

List of Figures

List of Tables

1. Introduction

The U.S. Army is interested in fast charging the most energy-dense lithium-ion batteries (LIBs) currently available—i.e., 18650 size with an Ampere hour (Ah) rating between 3.0 and 3.5 Ah. The common charging method currently used is a constant current–constant voltage (CC-CV) method that is very effective for nominal charging and usually takes about 1.5 h or more to achieve a 100% charge. When CC-CV charging is used for faster charging of LIBs (i.e., at twice the standard charging rate), studies and common understanding suggest it can reduce battery lifespan. Specifically, some sources indicate that when a battery's State of Health (SOH) is down to 80%, using fast charging can cause significant life-cycle reduction, with some studies suggesting a reduction of approximately 75%.[1] In this report, the CC-CV charging method will be compared with the sinusoidal ripple current average constant voltage (SRC-ACV) method. The SRC-ACV method is chosen because it allows the electrolyte to have a more equal distribution of ions[1] during the charging process, which should extend the LIB's lifetime and increase fast-charging efficiency. To evaluate this method the rate of charge will be three times the nominal charging rate for the LIBs under test, which equates to 3 C for 3000-mAh LIBs and 1.5 C for 3300- and 3500-mAh LIBs.

2. LIB Charging Perspective

LIB charging is a challenging process of electrochemical and physicochemical interactions with the lithium ion (Li+). Figure 1 displays an overall transition of the Li+ during charge from left to right, first being bonded in the commonly used material for the cathode of $LiCoO_2$ to being stored in the Li_xC_6 graphite anode. This process has ideal actions shown above the red dotted line and possible variations below it that have a degrading effect. To understand the charging process, the full transition has been divided into four sections (Figure 1A, B, C, and D).

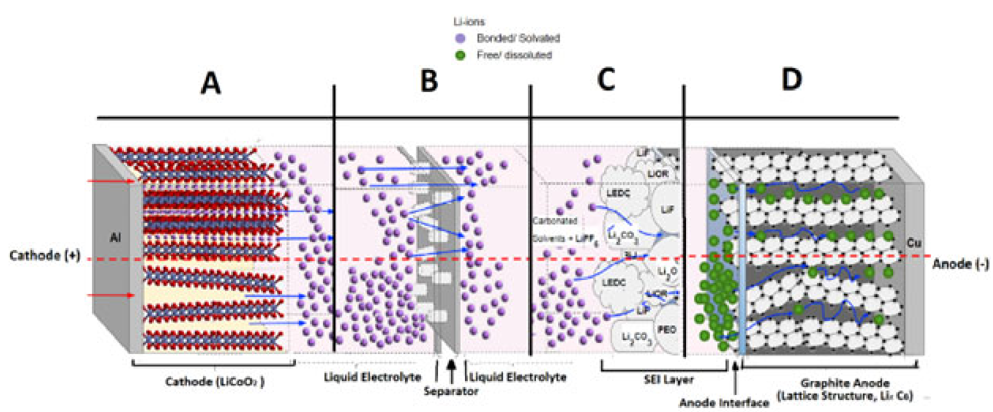

Figure 1. View of Li+ movement during charging.

Figure 1A focuses on extraction of the Li+ from the cathode—known as de-intercalation or de-lithiation. Ideally, the Li+ has a homogeneous distribution across the electrode allowing for reversible phase transition during normal charging rates without degradation (as illustrated above the red dotted line). Deformation of the structure caused by high rates of charge shown below the red dotted line makes the Li+ de-intercalation a nonreversible process, which produces a loss of active material and damages the cathode crystallinity produced by mechanical stress. Once the Li+ is de-intercalated from the cathode, solvation takes place in the liquid electrolyte and the Li+ is carried through the separator to the anode. The electrolyte solution is typically a mixture of carbonate solvents with salts such as $LiPF_6$. In Figure 1B, the solvated Li+ flows through the separator. Porosity of the separator is key for the Li+ flow rate during charging and discharging.

Figure 1C is where the de-solvation of the Li+ takes place at the solid electrolyte/electrode interface (SEI) layer. Ideally, only the de-solvated Li+ makes it to the anode crystal surface and everything else is blocked by the SEI layer. Under the red dotted line, a high flow rate of the Li+ will produce undesired conditions (e.g., restricted migration by formation of a large concentration gradient, SEI formation, Li-plating, byproduct formation, and blocked electrode pores).

Figure 1D shows Li+ intercalation into the anode structure, diffusion in the anode structure, and bonding to form the intercalated phase. The crystal structure volume should be nearly constant, allowing for easier transport and the thermodynamically stable stage 1 composition of one Li+ per six carbons to be reached. Numerous other issues can interfere with anode intercalation—such as particle morphology or particle size, electrode porosity, graphite structure, electrolyte transport properties, and any lithium plating that has occurred on the anode surface leading to thickened SEI.[2–5]

The intercalation of the de-solvated Li+ is shown in more detail in Figure 2 with sections E, F, G, H, and I demonstrating the processes of intercalation, plating, and re-intercalation. Figure 2E occurs when the dissolved Li+ (shown in green), flow rate is reasonable, and intercalation takes place at the rate of Li+ arrival. This is the case for nominal or slow charge rates. When the Li+ flow rate is high, the graphite particles at the electrode surface may become fully intercalated and no longer accept lithium for intercalation, at which point lithium begins to plate on top of the anode (as shown in red in Figure 2F). Dendrites on the anode surface form (Figure 2G) as Li+ flow continues. If Li+ flow diminishes or ends (Figure 2H) the plated Li+ will then begin redistribution in the electrode (as shown in blue of Figure 2I). Redistribution is caused by the potential difference between the plated Li+ and partially intercalated graphite anode. Ideally, this process reduces the plated lithium until it is fully absorbed into the electrode structure. The plated lithium is highly reactive toward the electrolyte; therefore, some is inevitably consumed, which permanently reduces the capacity of the battery.[3–5]

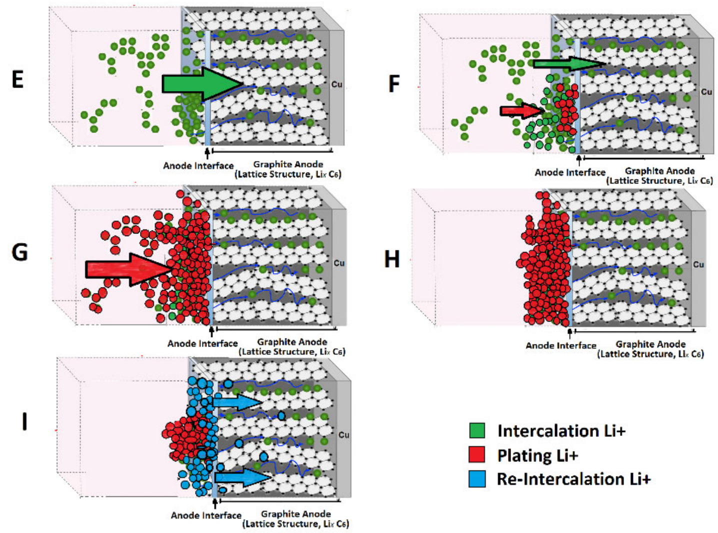

Figure 2. Intercalation, plating, and re-intercalation during a charge.

3. Charge Methods

Basic LIB charging begins with a CC.[6] A pulsed method usually uses a 50% duty-cycle pulse; therefore, it requires the amplitude of the pulse to be twice that of the CC level to charge at the same rate. Using an SRC waveform for charging the battery is like using a 50% duty-cycle pulse, requiring an amplitude twice the CC value. Figure 3 compares a 10-A charge rate for the CC, pulse, and SRC methods.[7] This gives the battery's voltage a sinewave at constant amplitude with the midpoint increasing as the charge is stored. The second charging method is CV. The CV charge step for LIB cells is set at 4.2 V to prevent cell damage as many commercial electrolytes begin to decompose at potentials above this value. To maintain a CV, the current is decreased and charging stops at a chosen current level or time. In the SRC method, when the midpoint of the cell's voltage is 4.2 V it then keeps the average voltage of a cycle at 4.2 V—this is known as ACV current. Figure 4 shows the voltage and current pattern of the CC-CV and SRC-ACV charge methods with the CC portion in the gray area. The ripple of the SRC-ACV method is 1 kHz because that is the frequency used to determine the impedance of LIBs.[8–10] For batteries being charged at 3 C the set charging time is 20 min and for those being charged at 1.5 C the charging time is 40 min. This will complete charging during the ACV and CV well before the current gets to 500 mA. This method does not fully charge the battery; however, we will show charging efficiency and SOH performance differences between the methods.

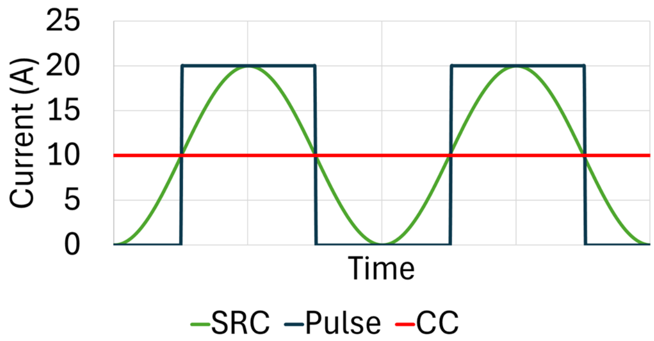

Figure 3. **Comparison of CC, pulse, and SRC methods.**

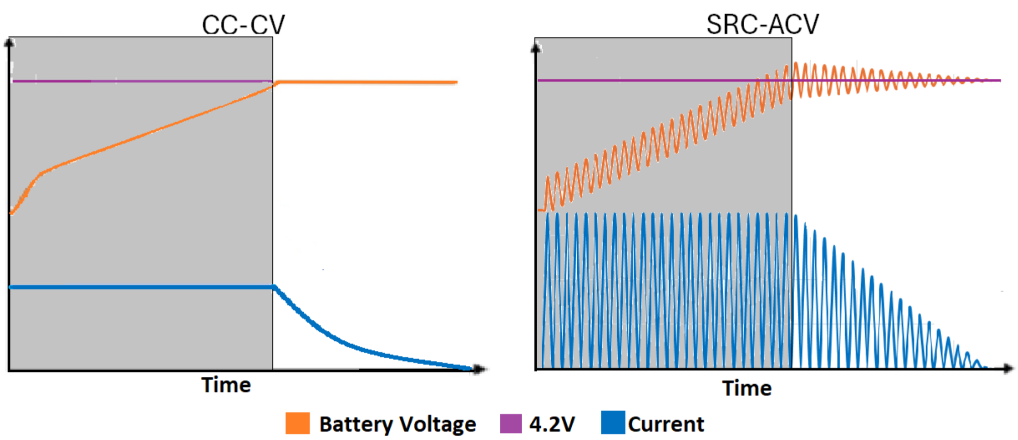

Figure 4. **SRC-ACV and CC-CV charging methods.**

4. SRC-ACV Source

The direct variable current converter (DVCC) was developed to be capable of implementing the SRC-ACV charging methodology. The operational layout of the DVCC is shown in Figure 5. The amplitude of the sinewave is set for twice the desired charging current and the battery voltage is read by the microcontroller to adjust the offset of the sinewave during the SRC period. During the ACV period, the offset is constant, and the amplitude of the sinewave is decreased to keep the midpoint of the battery voltage at 4.2 V. The microcontroller delivers the sinusoidal waveform values by an 8-bit parallel output to the digital-to-analog converter (DAC). The DAC produces V_{sin}, which is compared with the 250-kHz triangular waveform at the comparator that outputs V_{pwm} to drive the buck DC–DC converter. An Agilent 6038A DC power supply feeds the DVCC with 15 V; thus, enabling it to provide an SRC-ACV charge with an amplitude of 40 A.

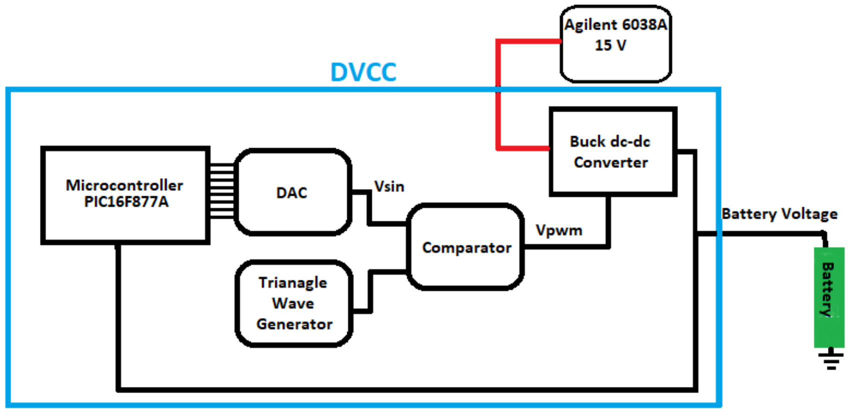

Figure 5. Pulse-width modulation generator.

5. Test Setup

The five different 18650 LIBs that were tested all have a standard charge rate of 0.5 C and are listed in Table 1. Each model was tested as a pair: one cell charged using the CC-CV method and the other with the SRC-ACV method. The 3300- and 3500-mAh cells (i.e., high-energy cells), were chosen for their energy density benefits. The 3000-mAh cells (i.e., high-power cells), were chosen for their power density benefits. Table 1 shows that the calculated power density provided by the high-power cells is greater than twice the calculated power density of the high-energy cells while only lacking a maximum of 20% in energy density.

Table 1. Lithium-ion cells used for testing.

18650 batteries						
	Manufacturer	**Model**	**mAh**	**Weight (g)**	**W/kg**	**Wh/kg**
High-energy	LG	INR18650-MJ1	3500	49	293.8	257
	Molicel	INR18650-M35A	3500	45	320	278
	Sanyo	NCR18650GA	3300	48	300	247
High-power	Epoch	18650-3000P	3000	45	800	240
	Samsung	INR18650-30Q	3000	48	750	225

Figure 6 shows the testing layout where the Peripheral Interface Controller (PIC) Control Board regulates the individual load banks (DL3021) and relays (W389CK-12 and W389CK-2) in addition to the DVCC. The Agilent E3633A power supply remains active throughout the battery cell testing. Charging begins and ends with the operation of the relays. The W389CK-2 relays are used so that the batteries are only connected to voltage monitors with a resistance of 50 kΩ during the resting period. The batteries are individually monitored by temperature probes while they are in an externally vented chamber. The test cycle procedure for the LIBs lasts approximately 122 min per cycle for high-energy cells and approximately 68 min per cycle for high-power cells (Table 2).

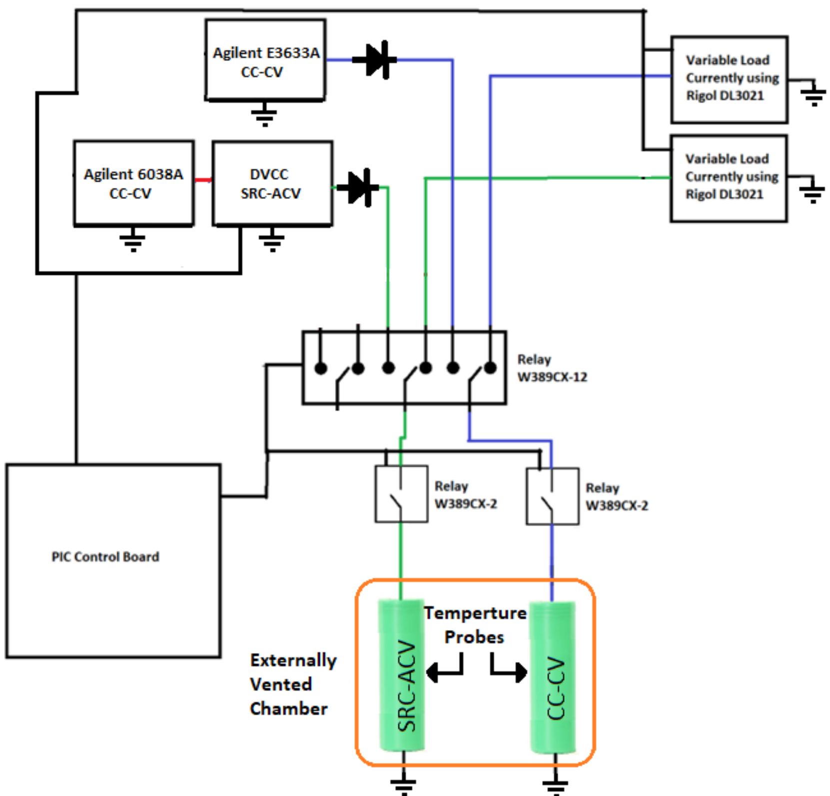

Figure 6. Fast-charging test layout.

Table 2. Cell test cycle.

Function	High-energy cells Time (min)	High-power cells Time (min)
1. Discharge batteries	~20	~10
2. Rest	20	20
3. Charge	40 at 1.5 C	20 at 3 C
4. Rest	10	10
5. Independent discharge—stops when it reaches 2.5 V	<52 at 4 A (1.14 C)	<18 at 10 A (3.33 C)
6. Return to step 2 for 200 cycles	. . .	. . .

6. Test Results

The following results highlight the diverse characteristics in the charging and discharging performance of the CC-CV and SRC-ACV methodologies. Each LIB was subjected to the cycles described in Table 2. In the following figures, time of constant current period between initial and final charging cycle, SOH through completed cycles, and difference of SOH between charging methods are presented. The cells' temperature for each method did not have more than 5 C difference throughout the charging cycles.

6.1 LG INR18650-MJ1 3500 mAh

The LG INR18650-MJ1 completed a total of 81 testing cycles. The charging response of the cells was compared at the 1st and 81st testing cycles. Using the CC-CV or SRC-ACV charging methodologies shown in Figures 7 and 8, we see that the SRC portion of the charging is longer than the CC portion. This difference is approximately 5 min in the 1st charge cycle with the CC lasting 25 min and the SRC lasting 29 min; the difference is approximately 2 min in the 81st charge cycle with the CC lasting 10.8 min and the SRC lasting 12.5 min (as indicated by the red arrows).

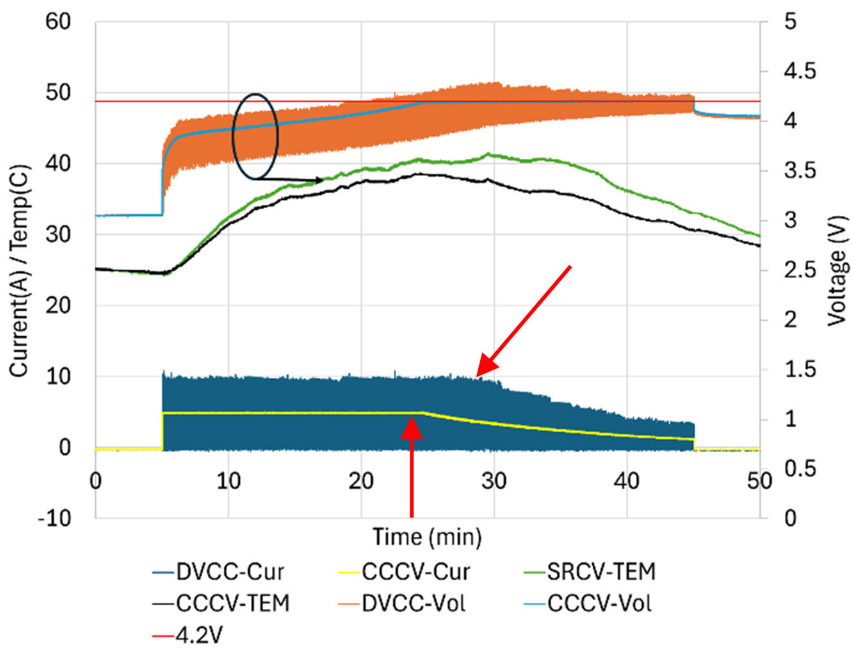

Figure 7. First SRC-ACV and CC-CV charge cycle of LG INR18650-MJ1.

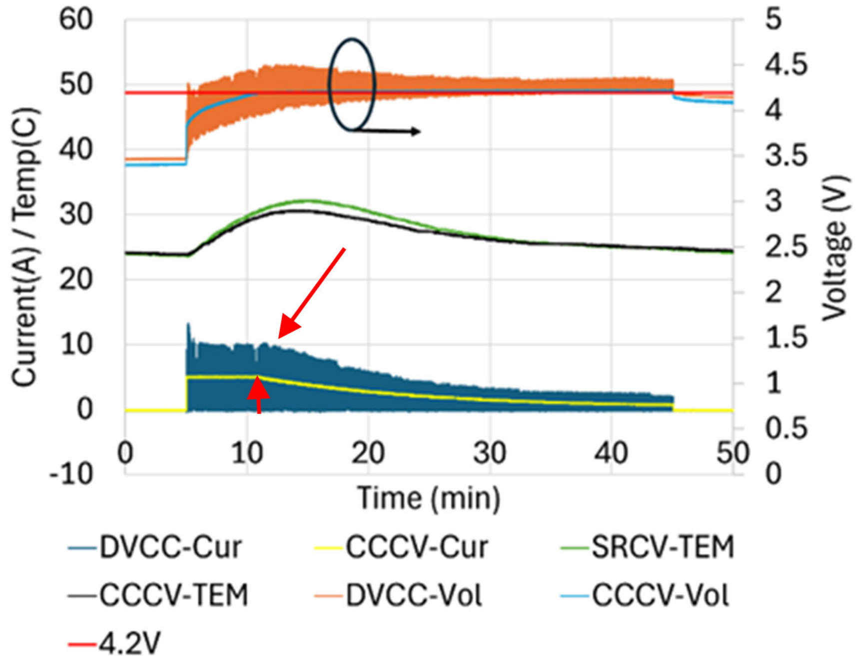

Figure 8. 81st SRC-ACV and CC-CV charge cycle of LG INR18650-MJ1.

The resulting SOC from the charging methods through 81 cycles is shown in Figure 9 with the green line representing the level of an average 20% reduction from the initial SOC, which was reached at 53 cycles for the CC-CV cell and 57 for the SRC-ACV cell. Figure 10 shows that the SRC-ACV SOC is greater for the first 20 cycles by an average of 2.5%.

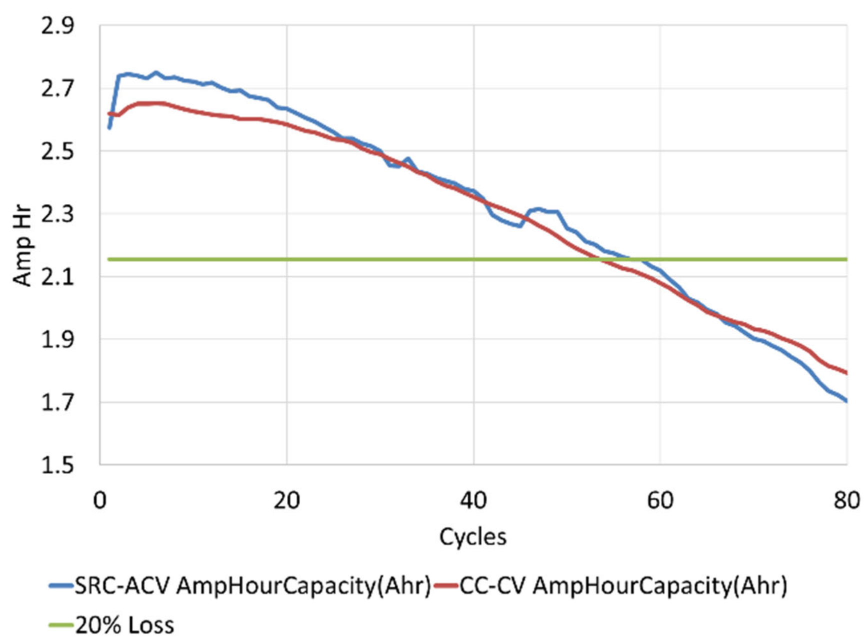

Figure 9. SOC degradation per cycle for LG INR18650-MJ1.

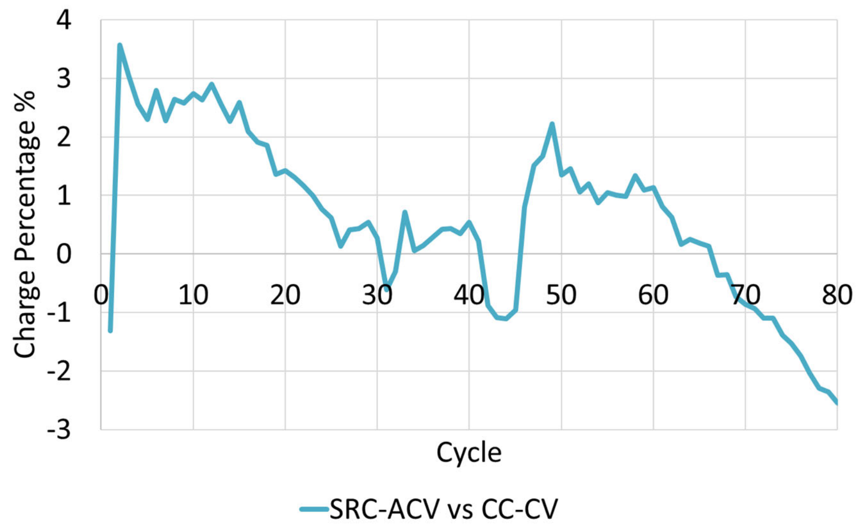

Figure 10. SOC percentage difference between SRC-ACV and CC-CV for LG INR18650-MJ1.

6.2 Molicel INR18650-M35A 3500 mAh

The Molicel INR18650-M35A completed a total of 187 cycles. The 1st and 187th charging of the CC-CV and SRC-ACV methods are compared in Figures 11 and 12, respectively, showing that the SRC charging portion is longer than the CC portion. This difference is about 4 min in the 1st charging with the CC lasting 24.7 min and the SRC lasting 28.85 min; it is approximately 7 min in the 184th charging with the CC lasting 7.98 min and the SRC lasting 15 min (as indicated by the red arrows).

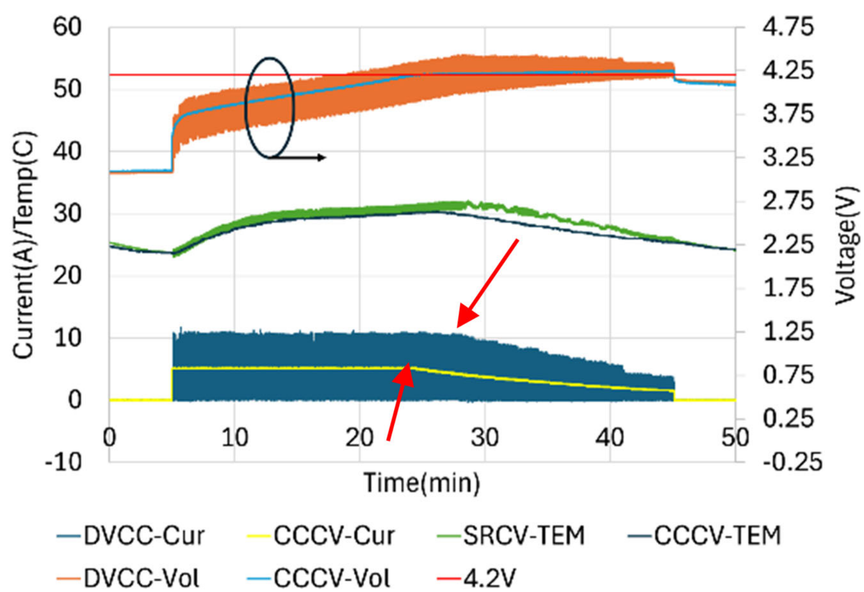

Figure 11. First SRC-ACV and CC-CV charge of Molicel INR18650-M35.

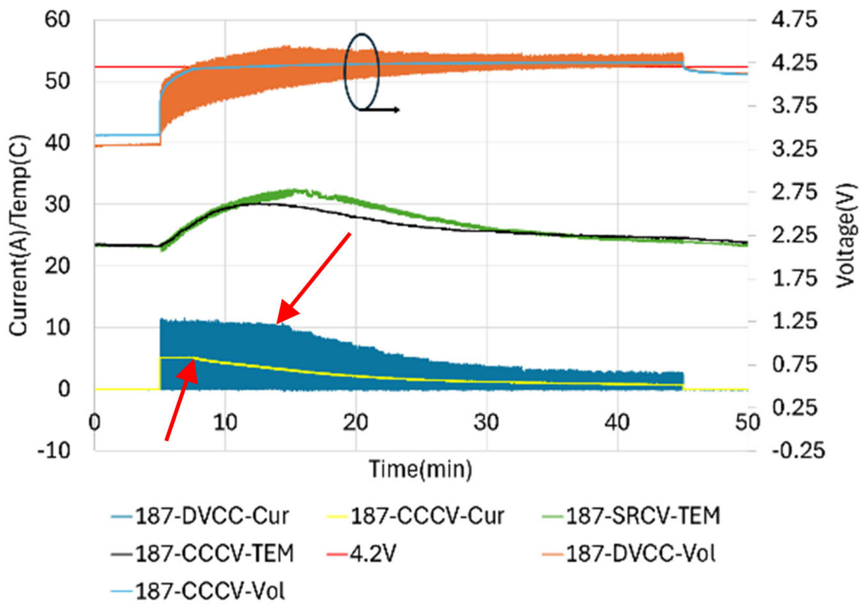

Figure 12. 187th SRC-ACV and CC-CV charge of Molicel INR18650-M35A.

The resulting SOC from 180 cycles is shown in Figure 13 with the green line representing the level of an average 20% reduction from the initial SOC, which was reached at 105 cycles for the CC-CV cell and 146 for the SRC-ACV cell. During the 146 cycles of the SRC-ACV method the difference in SOC varied between 1.1% and 7.8% (Figure 14).

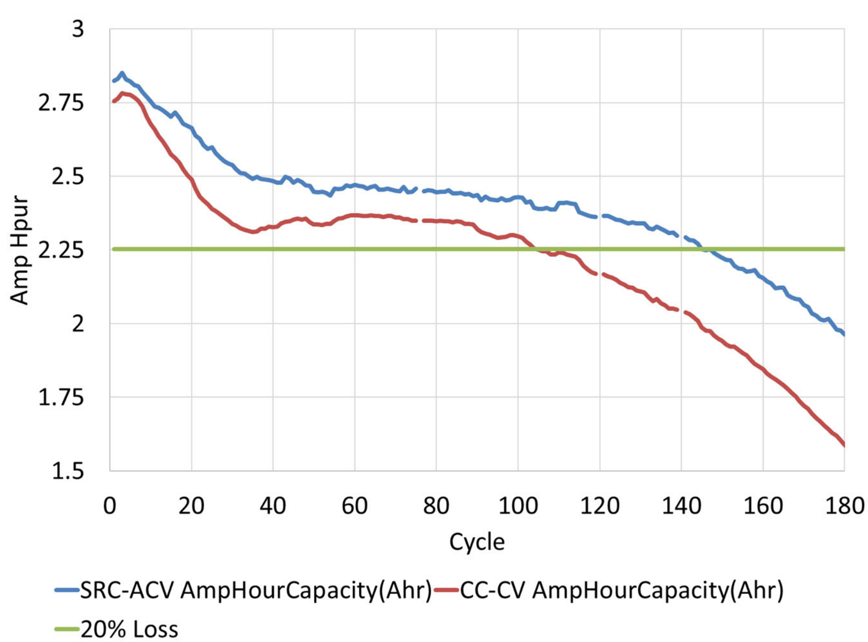

Figure 13. SOC degradation for Molicel M35A.

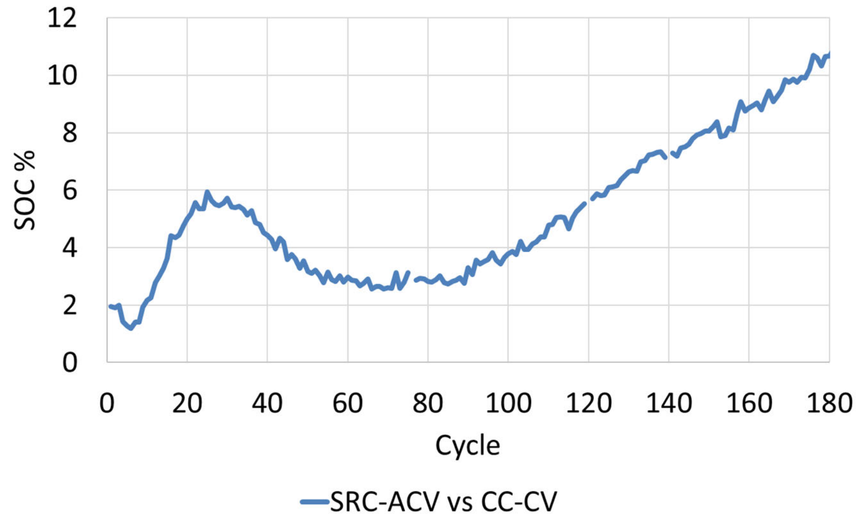

Figure 14. SOC difference between SRC-ACV and CC-CV for Molicel M35A.

6.3 Sanyo NCR18650GA 3300 mAh

The Sanyo NCR18650GA model completed 35 charge cycles. The 1st and 35th charging of the CC-CV and SRC-ACV methods are compared in Figures 15 and 16, respectively, showing that the SRC portion of charge is longer than the CC portion. This difference is about 5.5 min in the 1st charge with the CC lasting 24.7 min and the SRC lasting 30 min, and approximately 2.5 min in the 35th charge with the CC lasting 8.2 min and the SRC lasting 10.7 min (as indicated by the red arrows).

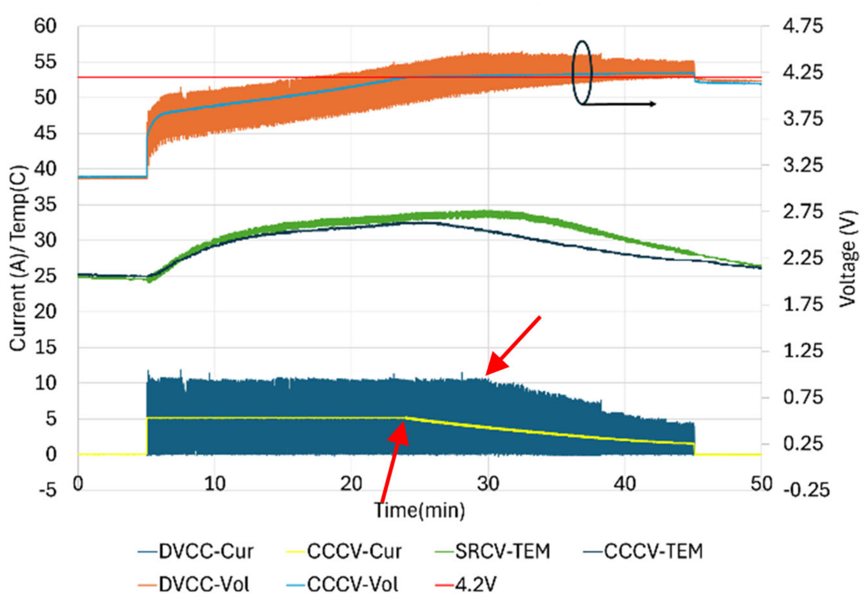

Figure 15. First SRC-ACV and CC-CV charge of Sanyo NCR18650GA.

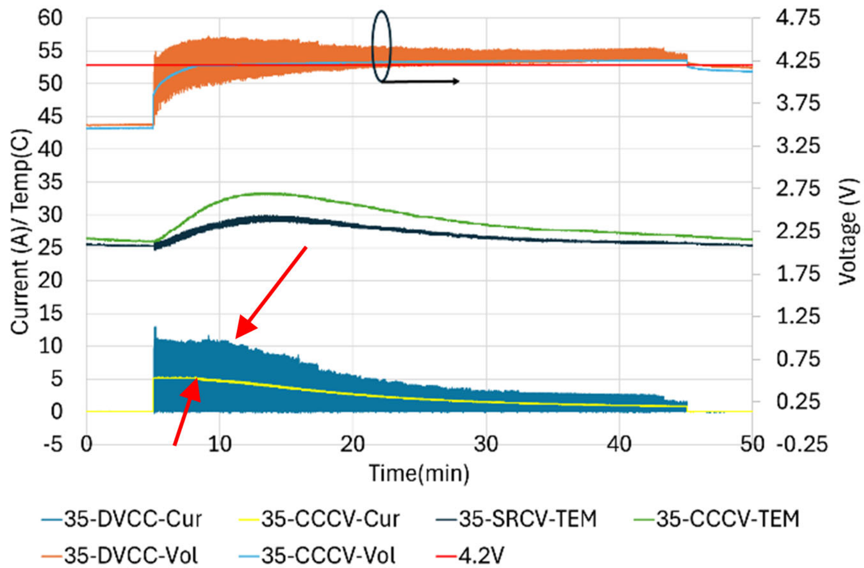

Figure 16. 35th SRC-ACV and CC-CV charge of Sanyo NCR18650GA.

After only 15 cycles both the CC-CV and SRC-ACV cells lost 20% SOC (Figure 17). Figure 18 shows that up until the 20% SOC was lost, the SRC-ACV method maintained a better charge efficiency.

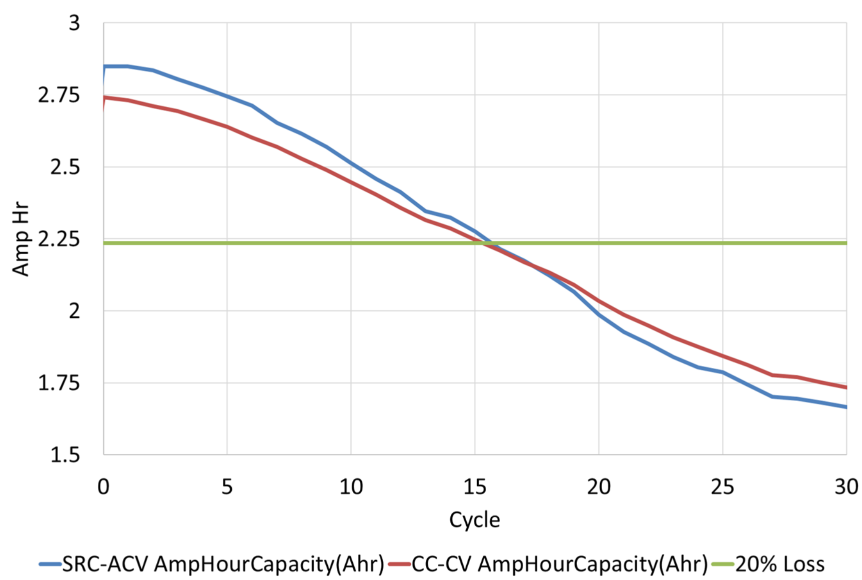

Figure 17. SOC per cycle for Sanyo NCR18650GA.

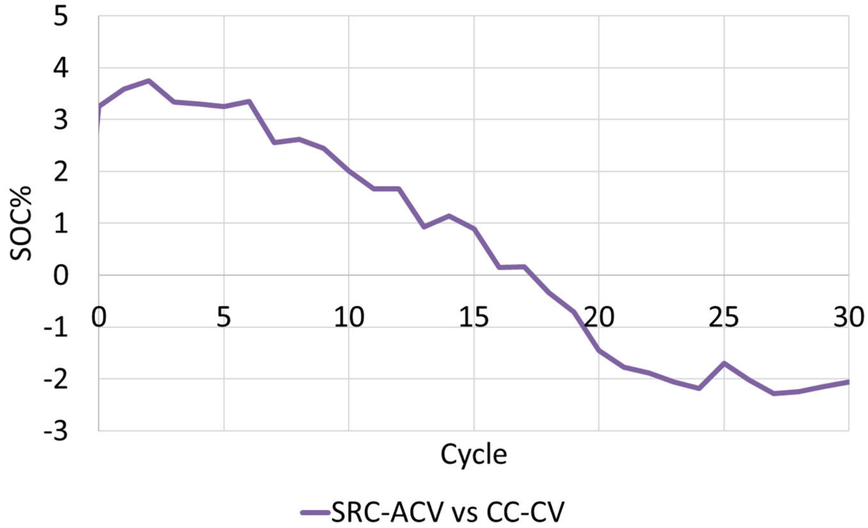

Figure 18. SOC percentage difference between SRC-ACV and CC-CV for Sanyo NCR 18650GA.

6.4 Epoch 18650HJ2

The Epoch 18650HJ2 model completed 220 charge cycles. The 1st and 220th charging of the CC-CV and SRC-ACV methods are compared in Figures 19 and 20, respectively, showing that the SRC portion of charge is longer than the CC portion. This difference is approximately 3 min in the 1st charge with the CC lasting 11.4 min and the SRC lasting 14.1 min, and less than 1 min in the 220th with the CC lasting 9.5 min and the SRC lasting 9.9 min (as indicated by the red arrows).

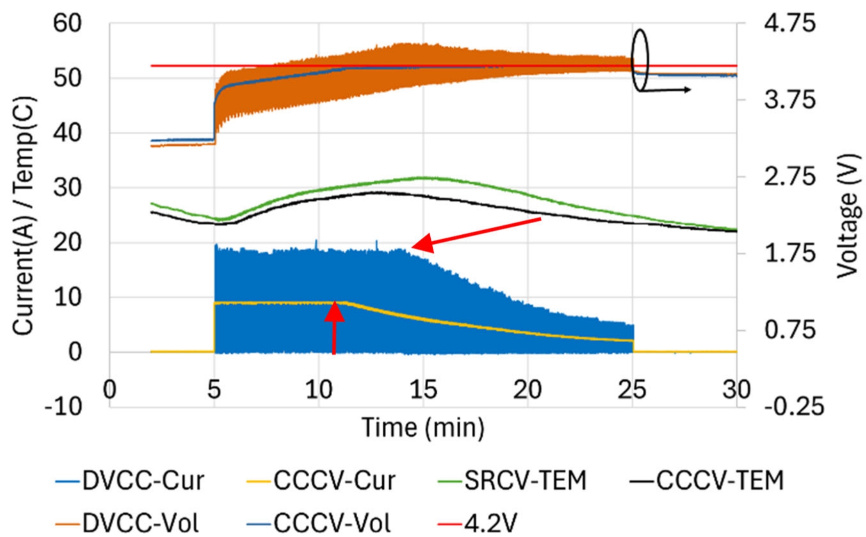

Figure 19. First SRC-ACV and CC-CV 3 C charging of Epoch 18650HJ2.

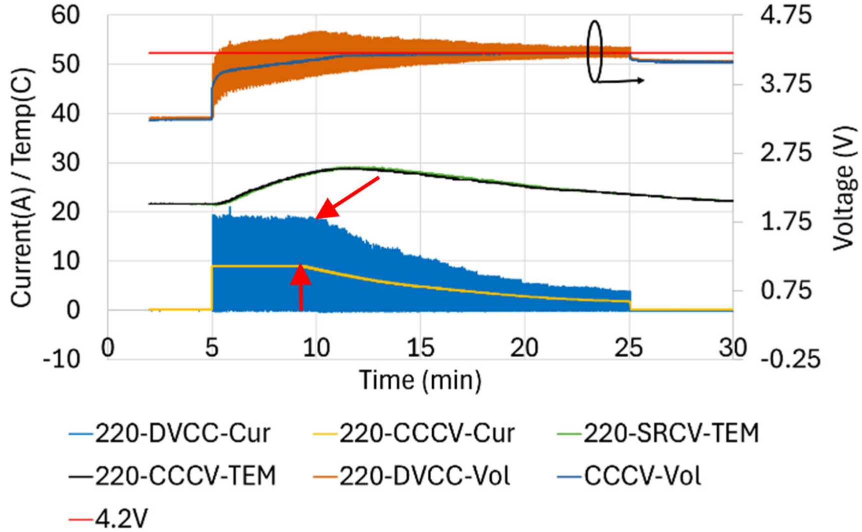

Figure 20. 220th SRC-ACV and CC-CV 3 C charging of Epoch 18650HJ2.

Both methods of charging lasted beyond 200 cycles before reaching the 20% lost threshold (Figure 21). During the first 90 cycles the cell using the SRC-ACV method SOC was at least 4.5% greater than the CC-CV method cell (Figure 22). From cycle 90 to 200 the difference decreased roughly at 0.04% SOC per cycle rate.

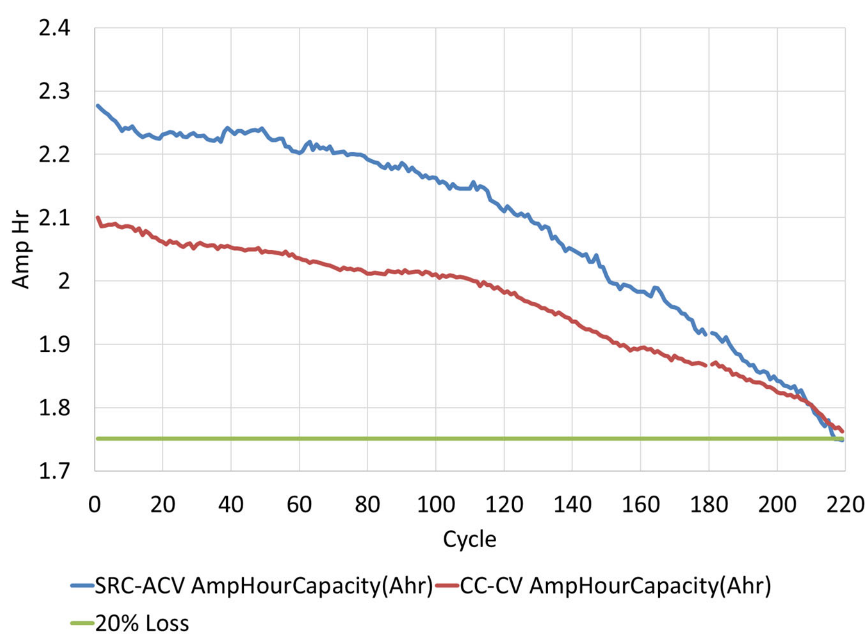

Figure 21. SOC degradation between SRC-ACV and CC-CV for Epoch INR18650HJ2.

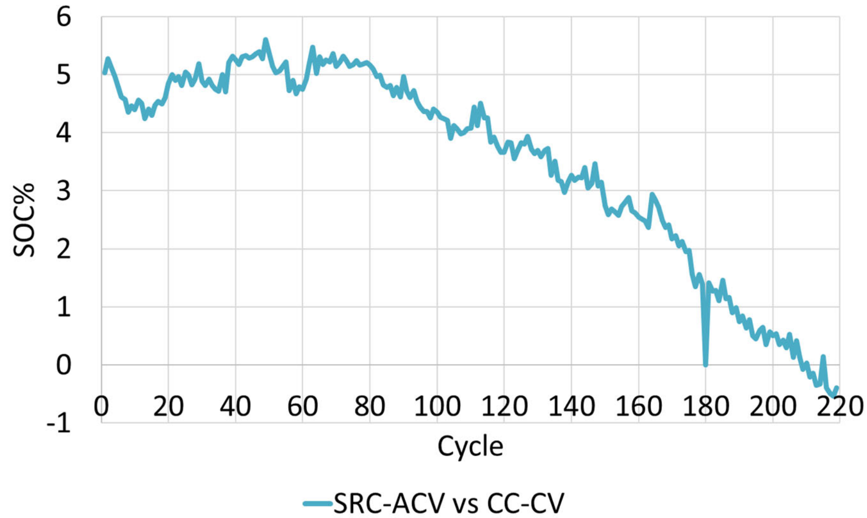

Figure 22. SOC difference between SRC-ACV and CC-CV for Epoch INR18650HJ2.

6.5 Samsung INR18650-30Q

The Samsung INR18650-30Q model completed a total of 507 charge cycles with a 3-h rest between cycles 277 and 278. The 1st and 277th charging of the CC-CV and SRC-ACV methods are compared in Figures 23 and 24, respectively, showing that the SRC portion of charge is longer than the CC portion. This difference is about 3.5 min in the 1st charge with the CC lasting 8.8 min and the SRC lasting 12.3 min, and less than 1 min in the 277th with the CC lasting 9.2 min and the SRC lasting 10 min (as indicated by the red arrows).

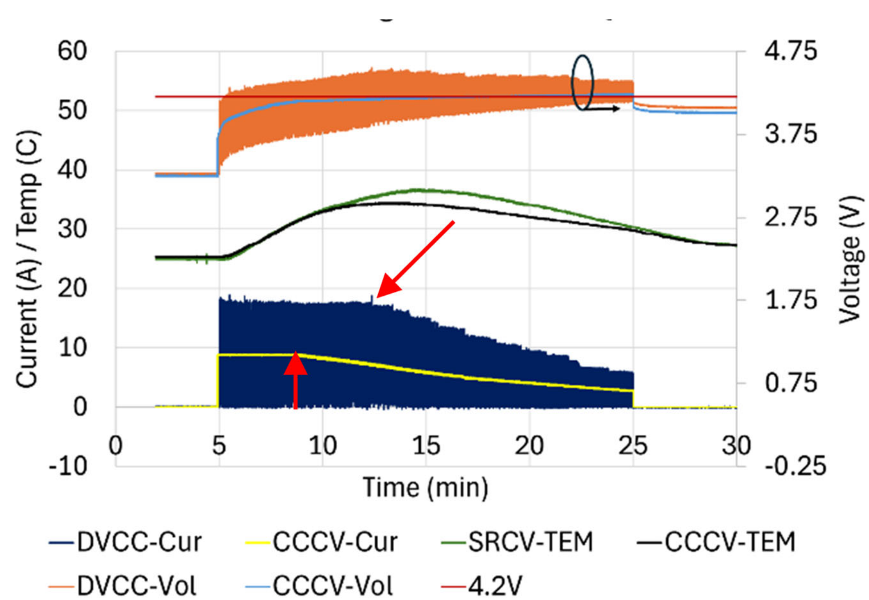

Figure 23. INR18650-30Q first charge cycle of SRC-ACV and CC-CV at 3 C.

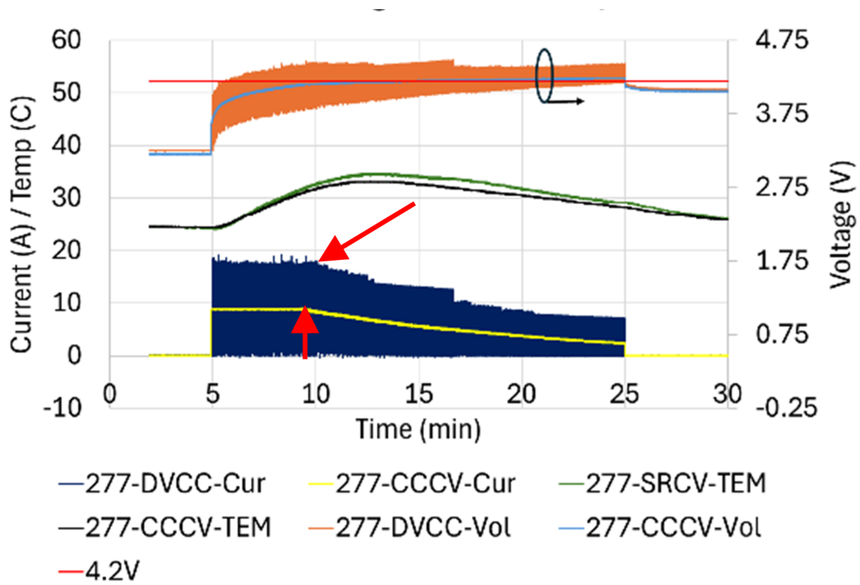

Figure 24. INR18650-30Q 277th charge cycle of SRC-ACV and CC-CV at 3 C.

Figure 25 shows that neither charge method's cell SOC decreased past the 20% threshold before 277 cycles with the CC-CV falling 7% and the SRC-ACV falling 11%. The cells were at rest for approximately 3 h before completing another 230 cycles with the SOC diminishing only 3% for the CC-CV and 3.4% for the SRC-ACV cells. After the rest, note that the SOC increased slightly at 2.5% for the SRC-ACV cell and 1.3% for the CC-CV cell. Figure 26 shows that throughout the cycles the SRC-ACV cell maintained greater SOC than the CC-CV cell and for the first 70 cycles it was greater than 3%.

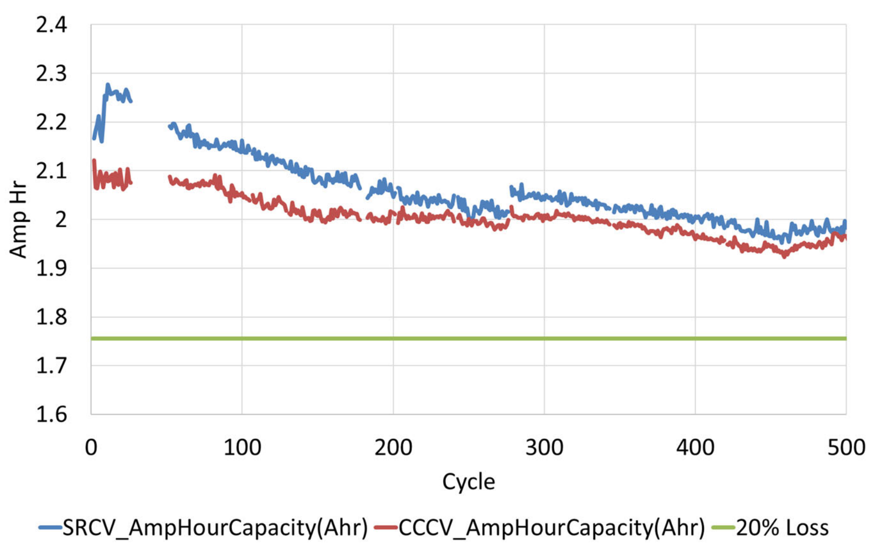

Figure 25. SOC after 20 min 3 C charge rate for INR18650-30Q.

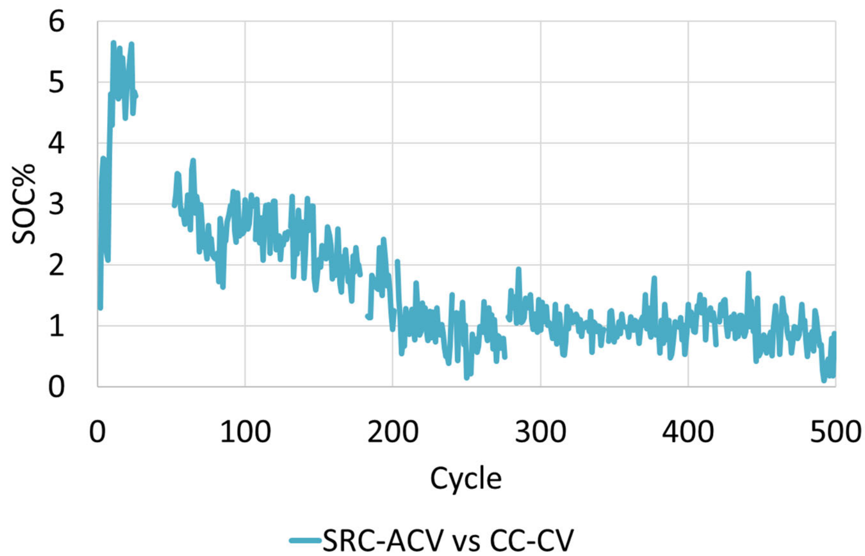

Figure 26. SOC difference between SRC-ACV and CC-CV for INR18650-30Q.

7. Conclusion

The cycle length for the tested cells before diminishing 20% is shown in Table 3. The longest cell of 3500-mAh cycled was the Molicel INR18650-M35A where the SRC-ACV provided 144 cycles, which was 39 more cycles than the CC-CV method. The 3300-mAh Sanyo NCR18650GA was the lowest; it was only able to reach 16 cycles for each method. The 3000-mAh cells were both able to pass the 200-cycle mark with the Samsung INR18650-30Q greatly surpassing it with 277 cycles in the uninterrupted format without reaching the 20% loss level. With all cells the SRC-ACV method provided a 3%–6% more-efficient charge performance, which could be significant depending on the application. From the SOC graphs it can be seen that the SRC-ACV method causes slightly steeper degradation through the cycles. The steeper degradation may be the result of the cell's higher-energy transaction through each cycle. This could only be confirmed by testing more cells with these charging methods.

Table 3. Cycles before 20% SOC degradation.

Manufacturer	Model	mAh	CC-CV	SRC-ACV
LG	INR18650-MJ1	3500	54	57
Molicel	INR18650-M35A	3500	105	144
Sanyo	NCR18650GA	3300	16	16
Epoch	18650-3000P	3000	220	219
Samsung	INR18650-30Q	3000	>277	>277

8. References

1. Chen L-R, Wu S-L, Shieh D-T, Chen TS-R. Sinusoidal-ripple-current charging strategy and optimal charging frequency study for Li-ion batteries. IEEE Transactions on Industrial Electronics. 2013;60(1).

2. Thusitha Asela Bandara TG, Viera JC, González M. The next generation of fast charging methods for lithium-ion batteries: the natural current-absorption methods. Renewable and Sustainable Energy Reviews. 2022;162:112338.

3. Qianqian L et al. Understanding undesirable anode lithium plating issues in lithium-ion batteries. RSC Adv. 2016;6:88683.

4. Tomaszewska A et al. Lithium-ion battery fast charging: a review. eTransportation. 2019;1:100011.

5. Agubra VA, Fergus JW. The formation and stability of the solid electrolyte interface on the graphite anode. Journal of Power Sources. 2014;268:153–162.

6. Yina Y et al. New fast charging method of lithium-ion batteries based on a reduced order electrochemical model considering side reaction. Journal of Power Sources. 2019;423:367–379.

7. Huang X, Jin S, Meng J, Teodorescu R, Stroe D-I. The effect of pulsed current on the lifetime of lithium-ion batteries. IEEE Energy Conversion Congress and Exposition. 2021.

8. Wassiliadis N et al. Review of fast charging strategies for lithium-ion battery systems and their applicability for battery electric vehicles. Journal of Energy Storage. 2021;44:103306.

9. Huang X et al. A review of pulsed current technique for lithium-ion batteries. Energies. 2020;13.

10. Hemavathi S, Shinisha A. A study on trends and developments in electric vehicle charging technologies. Journal of Energy Storage. 2022;52:105013.

List of Symbols, Abbreviations, and Acronyms

ACV	Average Constant Voltage
Ah	Ampere Hour
CC	Constant Current
CC-CV	Constant Current–Constant Voltage
CV	Constant Voltage
DAC	Digital-to-Analog Converter
DC	Direct Current
DVCC	Direct Variable Current Converter
Li+	Lithium Ion
LIB	Lithium-Ion Battery
PIC	Peripheral Interface Controller
SEI	Solid Electrolyte/Electrode Interface
SOH	State of Health
SRC	Sinusoidal Ripple Current

1 (PDF)	DEFENSE TECHNICAL INFORMATION CTR DTIC OCA
1 (PDF)	DEVCOM ARL FCDD RLB CB TECH LIB